Chemical Science

ROYAL SOCIETY OF CHEMISTRY

EDGE ARTICLE

View Article Online
View Journal | View Issue



Cite this: *Chem. Sci.*, 2025, **16**, 7039

All publication charges for this article have been paid for by the Royal Society of Chemistry



# Decoding growth inhibitory associated pathways of xenometal–siderophore antibiotic conjugates in *S. aureus*†

Axia Marlin,*[ab] Minhua Cao,[ab] Joelle El Hamouche,[a] Owen Glaser[ab] and Eszter Boros *[ab]

Received 17th December 2024
Accepted 15th March 2025

DOI: 10.1039/d4sc08509d

rsc.li/chemical-science

Pathogenic *Staphylococcus aureus* causes most infectious disease related deaths in the developed world. Continuously evolving resistance to clinically approved antibiotics and combination therapies limits treatment efficacy; new strategies that evade and slow resistance or produce resistant mutants with reduced fitness are needed. We employ antibiotics conjugated to bacterially recognized siderophores to potentiate their efficacy. Acting as a Trojan horse, the siderophore antibiotic conjugates efficiently deliver the antibiotic inside the bacterial cytoplasm by hijacking the iron transport system pathways which are crucial for bacterial survival. Here, we investigated the mechanism of action of gallium xenometallomycins (siderophore antibiotic conjugates incorporating non-endogenous metal ions), **Ga–DFO–Cip** and **Ga–LDFC–Cip**, which have demonstrated high potency compared to the parent antibiotic's efficacy *in vitro* in *S. aureus* infection. Employing physicochemical, synthetic and transcriptomic analysis studies, this work reveals that kinetically inert, gallium-containing xenometallomycins targeting cytoplasmic bacterial targets impart differential resistance and gene expression profiles when compared to their parent antibiotic in *S. aureus* bacterial strains. Both **Ga–DFO–Cip** and **Ga–LDFC–Cip** effectively disrupt iron–siderophore biosynthesis and uptake machinery. We affirm our results with the radioactive surrogate $^{67/68}$**Ga–DFO–Cip** and demonstrate that the bacterial uptake in **Ga–DFO–Cip**-resistant *S. aureus* strains is impaired, leading to diminished compound accumulation *in vitro* and *in vivo*.

## Introduction

*S. aureus* (SA) is a Gram-positive pathogen that causes most of the severe and lethal hospital acquired infections in the developed world. This pathogen is responsible for fatal pathologies such as pneumonia, meningitis and toxic shock syndrome.[1–4] *S. aureus* infections remain challenging to treat because of the bacterium's ability to persist and adapt. Antibiotic overuse, rapid replication and evolution have promoted the emergence of drug resistant strains of *S. aureus* worldwide.[5,6] Therefore, new antibiotic treatment strategies represent an urgent clinical need.

Bacterial virulence is closely associated with the acquisition of essential nutrients such as iron. In human hosts, iron is tightly controlled when sequestered, transported, and stored. Thus, pathogenic bacteria must mobilize iron from their host environment for survival. To do so, most bacterial pathogens produce siderophores, iron-scavenging small molecules for iron sequestration and internalization.[7,8] The corresponding iron complexes are internalized *via* selective and active membrane transport. The siderophore uptake machinery of bacteria is complex and not yet fully understood; a growing number of membrane translocators have been characterized.[9–15]

The iron–siderophore mediated uptake pathway can provide selective delivery of antimicrobial agents. Antibiotics conjugated to siderophores take advantage of the bacterial iron assimilation pathway, enhancing uptake to potentiate the antibiotic's antibacterial effect (Fig. 1). Potent metal-free (apo-) and pro-drug versions of such siderophore–antibiotic conjugates were introduced by Miller and Nolan.[16,17] Cefiderocol, a bidentate catechol–cephalosporin conjugate, was approved by the Federal Drug Administration (FDA) in 2019 (for structures, see Fig. 2).[18–21]

The recognition and import of siderophore–antibiotic conjugates *via* selective transmembrane transport requires binding and transposition of a metal-bound species that closely mimics the iron complex. However, an increase in iron concentration in the bacterial growth media results in diminished potency of siderophore–antibiotic conjugates in *in vitro* assays.[22,23] Our group and others have shown that the

[a]*Department of Chemistry, Stony Brook University, Stony Brook, New York 11790, USA*
[b]*Department of Chemistry, University of Wisconsin-Madison, Madison, Wisconsin 53706, USA. E-mail: eboros@wisc.edu; amarlin@wisc.edu*

† Electronic supplementary information (ESI) available. See DOI: https://doi.org/10.1039/d4sc08509d

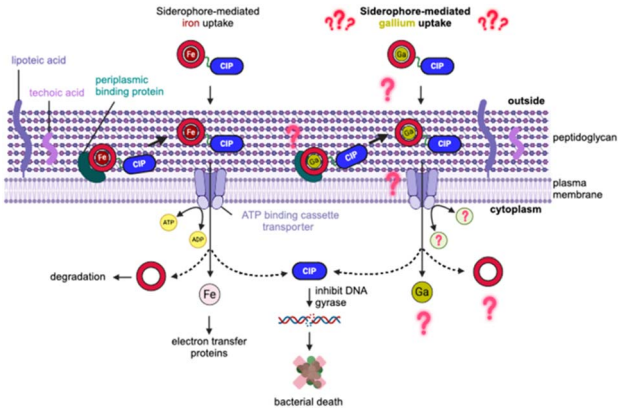


Fig. 1 Transport internalization pathway for gallium hydroxamate-type siderophore–ciprofloxacin conjugate in *wt S. aureus* using active uptake machinery. Gallium-mediated mode of action as well as ciprofloxacin-induced toxicity at the molecular level remains unknown and is the subject of this work.

displacement of Fe(III) by the non-endogenous xenometal Ga(III) not only recovers the growth inhibitory effect but can also significantly potentiate the corresponding siderophore–antibiotic drug conjugate.[24–29] Among xenometals of interest, Ga(III) represents the best Fe(III) mimic due to its comparable ionic radius (Ga: 0.76 A; Fe: 0.78 A) and chemical hardness $\eta$ (Ga: 17; Fe: 12).[30] Lack of redox activity under physiological conditions renders Ga(III) unable to recapitulate the biological function of Fe(II/III).

Our group has recently demonstrated that gallium–siderophore–ciprofloxacin (**Cip**) conjugates **Ga–DFO–Cip** and **Ga–LDFC–Cip** (Fig. 2) can outperform the parent antibiotic ciprofloxacin in inhibiting growth of *S. aureus in vitro* and *in vivo*.[31,32] While this finding is encouraging and motivates further structure–activity relationship (SAR) campaigns, the mechanism of action and source for potentiation of those xenosideromycins in *S. aureus* are not known (Fig. 1). Previous literature reports hypothesized that the therapeutic effect of Ga(III) compounds arises from Fe(III) substitution in iron-dependent cofactors involved in electron transport cascades and redox-dependent Fe(III) enzymes,[24,26,33] while others suggest that Ga(III) selectively alters cellular respiration processes.[34]

To further improve the *in vitro* potency and *in vivo* efficacy for *S. aureus* infection, a better understanding of the mechanism of action of this unique compound class is required. Specifically, (1) what role do complex inertness and thermodynamic stability play? (2) Is cytoplasmic delivery of Ga(III) required to enhance potency? (3) Does resistance to the parent antibiotic also confer resistance to xenometallomycins? (4) Does the presence of Ga produce unique transcriptomic profiles? (5) How do xenometallomycin-induced mutations impact compound internalization? In this study, we have compiled an extensive set of characterization data to address these questions within the context of *S. aureus* infection.

## Results and discussion

### Compound library – design and synthesis

To date, our group has focused on hydroxamate-based siderophores as they confer potency against *S. aureus* bacterial strains.[31,32,35] We selected deferoxamine (**DFO**) and desferrichrome (**DFC**) siderophore structures inspired by the natural product sideromycins, salmycin and albomycin; we previously hypothesized that these siderophores retain good affinity for Ga(III) when compared to Fe(III) and are comparatively straightforward to functionalize, using the natural product precedent as a molecular design road map. These conjugates have been shown to effectively retain and enhance the antibiotic potency of **Cip** in *S. aureus*. Chemical synthesis of **DFO–Cip** and **LDFC–Cip** (Fig. 2), two conjugates incorporating the fluoroquinolone antibiotic ciprofloxacin, was achieved in accordance with previously reported procedures.[31,32] Ciprofloxacin and other fluoroquinolone antibiotics rely on cytoplasmic delivery as they target the DNA-gyrase.[36–39] To probe the role of

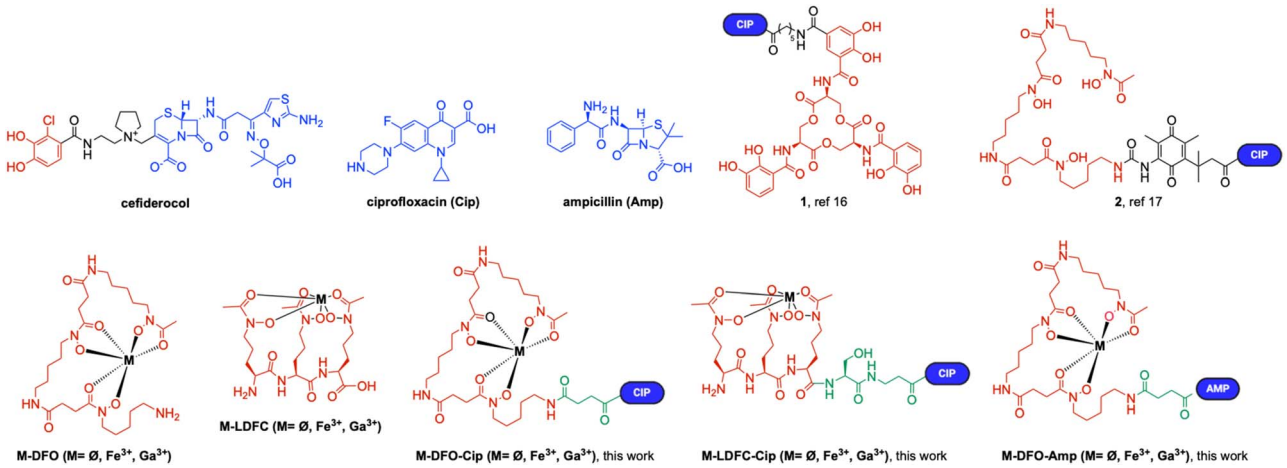


Fig. 2 Chemical structure of cefiderocol, an FDA approved siderophore–antibiotic conjugate, ciprofloxacin (**Cip**), previously investigated siderophore–antibiotic conjugates, and gallium-based compounds showing growth inhibitory effects on bacteria studied in this work. Red: siderophore, green: linker, and blue: ciprofloxacin or ampicillin.

the antibiotic, we synthesized the β-lactam containing, deferoxamine-linked ampicillin conjugate **DFO–Amp** (Fig. 2, for synthesis and characterization, see the ESI†). The chemical synthesis was conducted using sequential, solution-phase amide bond conjugations of building blocks. In our hands, incorporation of the siderophore building block was significantly improved by pre-chelation of Fe(III) or Ga(III), which efficiently masks the otherwise hydrolytically sensitive hydroxamate functional groups and reduces the number of steps to generate the final target construct.

### Relative stability of Ga(III) and Fe(III) complexes

To form sufficiently inert metal coordination complexes, the chelator must be carefully matched and selected according to the coordinative binding preferences, thermodynamic stability and pH dependent speciation of the corresponding metal ion. In contrast to non-metallated Trojan horse antibiotics such as cefiderocol, which relies on local Fe(III) pools at the site of infection to translocate to the bacterial periplasm,[40] xenometal cargos must be pre-chelated and form *in vivo* compatible, thermodynamically stable complexes. In this regard, hexadentate motifs are preferred over 4- or 2-dentate systems. Deferoxamine (**DFO**) and desferrichrome (**DFC**) form thermodynamically stable Fe(III) complexes as evidenced by reported $\log K$ values of 31.3 and 29.07 with **DFO** and **DFC** respectively. The gallium complexes have $\log K$ values of 28.65 and 27, respectively.[41–44] In addition to thermodynamic stability, high relative kinetic inertness is also desirable; as such, rapid dechelation to reach equilibrium would result in immediate loss of the metal payload *in vitro* and *in vivo*. To probe the effect of functionalization on the thermodynamic stability and kinetic inertness of the corresponding constructs, we conducted ligand exchange experiments with a 1000-fold excess of ethylenediaminetetraacetate (EDTA). Relative complex half-lives ($t_{1/2}$), rates of transchelation ($k_1$) and $K_{Fe}/K_{Ga}$ values are shown in Table 1, as determined by these transchelation experiments and derived from the thermodynamic stability constants for Fe(EDTA) and Ga(EDTA).[43]

In accordance with reported literature values for the corresponding thermodynamic stabilities of **DFO** and **DFC** complexes, we observe enhanced thermodynamic stability and kinetic inertness for Fe(III) complexes over Ga(III) complexes. However, functionalization of **DFO** complexes appears to reduce thermodynamic stability by 4 and 1 orders of magnitude for **DFO–Cip** and **LDFC–Cip** respectively. Our data set also demonstrates that kinetic inertness and thermodynamic stability are not correlated, with the **Fe–LDFC–Cip** complex showing rapid dechelation with half-lives of 10 minutes and below, whereas the **M–DFO–Cip** series exhibits improved inertness with 60–82 min half-lives. This corroborates previous kinetic inertness and metabolite analysis data obtained with radiochemically tagged analogues and metabolite analyses conducted previously.[31,32]

Table 1 Kinetic and thermodynamic stability values of the Fe(III) and Ga(III) complexes with DFO–Cip and LDFC–Cip

| | $t_{1/2}$ (min) | $k_1$ ($min^{-1}$) | $\log K_{LM}$ |
|---|---|---|---|
| **Fe–DFO–Cip** | 82.66 | $8.39 \times 10^{-3}$ | 26.89 |
| **Ga–DFO–Cip** | 60.81 | $1.14 \times 10^{-2}$ | 26.86 |
| **Fe–LDFC–Cip** | 10.34 | $6.70 \times 10^{-2}$ | 28.10 |
| **Ga–LDFC–Cip** | 57.96 | $1.20 \times 10^{-2}$ | 27.10 |

### Growth inhibition in *wt* and resistance induced *S. aureus*

The *in vitro* potency of the conjugates and their metal complexes was assessed by a conventional microbroth dilution assay, which quantifies the Minimum Inhibitory Concentration ($MIC_{98}$). The $MIC_{98}$ was recorded as the lowest compound concentration required to inhibit at least 98% of bacterial growth ($OD_{600} < 0.02$) at 16 hours of incubation in comparison to the $OD_{600}$ of the negative control wells (ESI eqn (1) and Section 3.2†).

To determine the impact of the metal chelator and ion separately from the conjugate constructs, we measured the growth inhibitory action of the metal ion citrate salts and siderophore complexes separately (ESI Fig. S23†). In accordance with our previous work on **Ga–LDFC** and **Ga–DFO**, **Ga–DFC** complexes also do not show any significant growth inhibitory activity, indicating that incorporation of an antibiotic small molecule drug is required to harness metal-complex mediated potentiation of growth inhibitory action. Indeed, both **Ga–DFO–Cip** and **Ga–LDFC–Cip** show improved $MIC_{98}$ when compared with the parent antibiotic **Cip** targeting the cytoplasmic topoisomerase in *S. aureus* (Fig. 3, Table 2). The corresponding apo- and Fe(III) complexes show comparable or diminished potency, respectively. The **DFO–Amp** series, which incorporates the cell-wall targeting β-lactam ampicillin, recapitulated previous trends: **Ga–DFO–Amp** shows a significantly enhanced $MIC_{98}$ when compared to the corresponding **Fe–DFO–Amp** complex; however, both compounds remain orders of magnitude less potent when compared to the parent antibiotic.

To demonstrate that the co-delivery of both molecular components must occur *via* covalent linkage, we also probed the growth inhibitory activity of mixtures of non-functionalized complexes with the native drug. Under these conditions, mixtures of **Ga–DFO/Cip** and **Ga–LDFC/Cip** showed no enhanced growth inhibition but reproduced the growth inhibitory capacity of ciprofloxacin (ESI, Fig. S29, and S30†). It is plausible that the siderophore-mediated uptake of the construct increases the total accumulation of ciprofloxacin, resulting in a net increase in delivered antibiotics.

As a first approach to probe if ciprofloxacin and our synthetic constructs exerted growth inhibition using the same mechanisms, we generated **Cip**, **Ga–DFO–Cip**, and **Ga–LDFC–Cip** resistant *S. aureus* bacterial strains. This was achieved by culturing and repetitive passaging of *wt S. aureus* in the presence of increasing, sub-MIC amounts of the corresponding antibiotic agent under iron-limiting conditions.[45,46] Using this approach, we achieved an increase in the $MIC_{98}$ of each compound by at least two orders of magnitude within 2–10 passages (ESI Fig. S24–S26†). Ciprofloxacin resistance was established at a $MIC_{98}$ of 75 μM, compared to a $MIC_{98}$ of 0.94

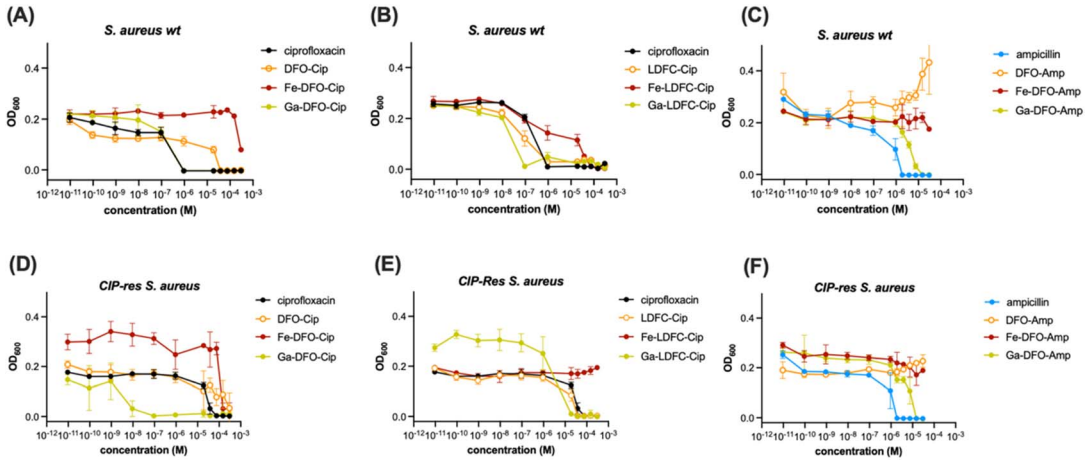


Fig. 3 Top panel: MIC assay plots of (A) **DFO–Cip** series, (B) **LDFC–Cip** series, and (C) **M–DFO–Amp** in *wt SA*. Bottom panel: MIC assay plots of (D) **DFO–Cip** series, (E) **LDFC–Cip** series and (F) **DFO–Amp** series in *Cip-Res SA*.

Table 2 Summary of $MIC_{98}$ (μM) determined in wt and resistant *S. aureus* strains for parent antibiotics and sideromycin complexes evaluated in this study. N/D = not determined; GP = growth promoting

| | *S. aureus* wt | *S. aureus* **Cip** res | *S. aureus* **Ga–DFO–Cip** res | *S. aureus* **Ga–LDFC–Cip** res |
|---|---|---|---|---|
| Ciprofloxacin (**Cip**) | 0.94 | 75 | 3.8 | 3.8 |
| Ampicillin (**Amp**) | 1.9 | 1.9 | 1.9 | 1.9 |
| **DFO–Cip** | 3.8 | 15 | >30 | 15 |
| **Fe–DFO–Cip** | 30 | 15 | >30 | 30 |
| **Ga–DFO–Cip** | ***0.94*** | ***0.094*** | 38 | 1.9 |
| **LDFC–Cip** | 15 | 7.5 | GP | N/D |
| **Fe–LDFC–Cip** | 7.5 | GP | GP | N/D |
| **Ga–LDFC–Cip** | ***0.094*** | 3.8 | 30 | 150 |
| **Fe–DFO–Amp** | 30 | GP | >30 | GP |
| **Ga–DFO–Amp** | 15 | 15 | 15 | 15 |

μM in the *wt S. aureus* strain (Table 2 and Fig. S24†). Similarly, the $MIC_{98}$ increased from 0.94 to 38 μM and 0.094 to 150 μM for **Ga–DFO–Cip** and **Ga–LDFC–Cip**, respectively (Table 2, Fig. S25 and S26†). These three strains subsequently provided the basis for the cross-resistance studies. Ciprofloxacin-resistant *S. aureus* (*S. aureus-Cip-res*) confers decreased efficacy of **Ga–LDFC–Cip** ($MIC_{98}$ = 3.8 μM), when compared to the *wt* strain, whereas the strain becomes sensitized to **Ga–DFO–Cip** ($MIC_{98}$ = 94 nM), indicating non-ciprofloxacin associated mechanisms of growth inhibition. The lack of cross-resistance indicates that resistance mechanisms that inhibit parent drug uptake do not correlate with those of the **Ga–DFO–Cip** conjugate. Control experiments with **DFO–Cip** and **Fe–DFO–Cip** indicate that Ga(III) is required to observe the enhanced potency, while ampicillin and **Ga–DFO–Amp** show no difference in efficacy. Conversely, the inverse relationship is not observed in cross-resistance experiments with the **Ga–DFO–Cip** resistant strain (*S. aureus GaDFO–Cip-res*), with **Cip** and **Ga–LDFC–Cip** also showing diminished potency (3.8 and 30 μM, respectively). Finally, the $MIC_{98}$ of **Ga–DFO–Cip** and **Cip** only decreases by 2–4-fold in efficacy in the **Ga–LDFC–Cip** resistant strain (*S. aureus GaLDFC–Cip-res*). Finally, the induced resistance mechanisms did not impact the potency of **Amp** or **Ga–DFO–Amp**. This further points to resistance mechanisms that do not impact bacterial cell wall composition or emergence of beta-lactamases.

### Transcriptomic analysis *via* RNA sequencing of *wt S. aureus* under iron-limited conditions

While induction of resistance in bacteria can provide insight into the mechanism of action of novel antibiotic drugs, we also sought to understand what biochemical signature each compound induced in treated *S. aureus*. To this end, we employed a bottom-up approach *via* RNA-Sequencing (RNA-Seq). RNA-Seq has become the gold standard tool to study the bacterial transcriptome.[47–50] Subjected to antibiotics at sub-MIC concentrations, extensive transcriptional changes can be detected to determine the impact of antibiotics on the expression of trans-membrane transport proteins, structural components of the bacterial cell envelope, DNA damage/repair mechanisms and nutrient homeostasis.

One of the challenges in implementing RNA-Seq for our compound class is introduced by iron-depleted assay conditions. This is employed to provide a more host-representative

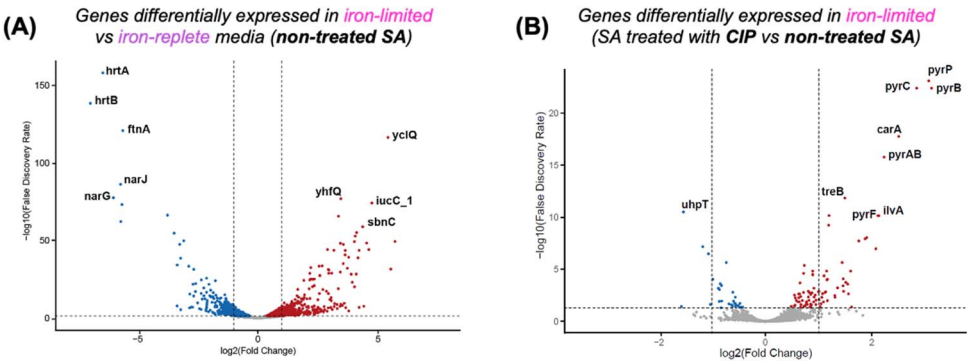


Fig. 4 Differential gene expression analysis in non-treated *S. aureus* (SA) or SA treated with ciprofloxacin. Significantly up- and down-regulated genes ($p < 0.05$) are shown in red and blue, respectively. Volcano plot of the genes that were differentially expressed in (A) iron limited *versus* iron replete media in non-treated SA or (B) SA treated with **Cip** under iron-limited conditions.

growth environment where metal ions, especially Fe(III), are tightly controlled. Therefore, we first probed changes in gene expression of *S. aureus* under iron-replete and iron-limited conditions. Differential gene expression analysis plots show the top significant differentially expressed genes with $p$ value < 0.05 experiencing up (red) or down (blue) regulation.

Fig. 4A shows gene expression changes of *S. aureus* under iron depletion alone. Our results indicate that the heme efflux ATPase system (*hrtA*/*hrtB*) and ferritin like protein (*ftnA*) (Fig. 4A) are downregulated to conserve iron resources within the bacterial cytoplasm.[51–53] Accordingly, Fe-dependent nitrate respiration is also downregulated (*narGJ*). Genes involved in endogenous siderophore synthesis (*sbnC*) and iron–siderophore uptake (*yclQ*/*yhfQ*) are upregulated (Fig. 4A). We next probed the effect of ciprofloxacin on gene expression in iron limited media. Complementary analysis of the differential expression levels further helps to distinguish effects induced by iron insufficiency *versus* those induced by the presence of ciprofloxacin, which binds DNA gyrase and inhibits topoisomerase IV.[36,38,39] As a part of the bacterial SOS responses activated by ciprofloxacin exposure, genes involved in pyrimidine biosynthesis (pyrAB, *pyrC*, *pyrB*, *pyrF*, and *pyrP*) are upregulated (Fig. 4B),[54–56] while hexose transport *via* the two-component pathway (*uhpABC*) that regulates the expression of the hexose phosphate transporter *uphT* is downregulated.[57–59] Treatment with ciprofloxacin decreases the *uhpT* gene transcription, suggesting that the bacteria are unable to maintain survival through hexose phosphate entry. In summary, these control data sets indicate that under iron-depleted conditions, ciprofloxacin down-regulates genes involved in nucleotide synthesis, while iron storage and iron acquisition are up-regulated in the background.

### Impact of xenometallomycins on *S. aureus* transcriptomics under iron-limiting conditions

Following our analysis of baseline transcriptomic changes in iron-depleted media, we conducted RNA-Seq analysis of *wt S. aureus* when exposed to sub-$MIC_{98}$ concentrations of the sideromycins and metal sideromycins. Following exposure to the **DFO–Cip** and **LDFC–Cip** compound series, we observed significant transcriptional changes that can be grouped into 8 broad categories including nucleotide metabolism, ribosomal activity, nitrate and amino acid metabolism, siderophore transport and biosynthesis, heme and saccharide transport. Fig. 5 summarizes our findings, with data grouped separately for the **DFO–Cip** and **LDFC–Cip** compound class and in direct comparison with ciprofloxacin. Genes responsible for protein expression that employ heme or other Fe-complexes as cofactors or substrates are highlighted in red. All compounds upregulate genes associated with the mechanism of action of ciprofloxacin under iron-restricted conditions, specifically nucleotide metabolism (*pyrB*, *pyrC*, *pyrP*, *pyrAB*, and *pyrF*) including *umuC*, a low-fidelity DNA polymerase as part of the SOS response commonly observed under fluoroquinolone stress.[60–62] All compounds also downregulate NADH-dependent formate dehydrogenase (*Fdh*), implicated in biofilm formation, and regulated down-stream by Fur under iron-limiting conditions (Fig. 5).[63]

Major differences are found in the presence of **Fe–DFO–Cip** and **Fe–LDFC–Cip** when compared with all other data sets. We observe decreased expression of siderophore transport, biosynthesis and heme import genes (*feuC*, *yusV*, *ylcQ*, *fhuD2*, *isdD*, *isdC*, and *isdE*), while iron storage genes, nitrogen metabolism (*narH*, *narG*, *nasD*, *nasF* and *narI*) and heme-dependent protein expression increase. These changes are notably absent in the presence of the apo-siderophores **DFO–Cip** and **LDFC–Cip** and diminished in the presence of **Ga–DFO–Cip** and **Ga–LDFC–Cip**. The introduction of the Fe-compounds mimics Fe-sufficient states, which downregulates endogenous siderophore production and uptake, rationalizing why we observe a decrease in efficacy of all Fe-complexes tested to date.

The RNA-Seq data set discussed does not single out differential up/down regulation of genes that arise uniquely in the presence of the gallium complexes. Few genes of interest indicate that the SOS response is activated in the presence of **Ga–DFO–Cip** (up-regulation of *lexA* and *umuC*). Both **Ga–DFO–Cip** and **Ga–LDFC–Cip** downregulate rplS (large ribosomal subunit protein bL19), which could indicate diminished efficacy in protein synthesis and thus decreased fitness. Diminished heme import (decrease in expression of *isdD*, *isdC*, and *isdB*), decrease in staphyloferrin synthesis (*sbnBCEH*) paired with retained

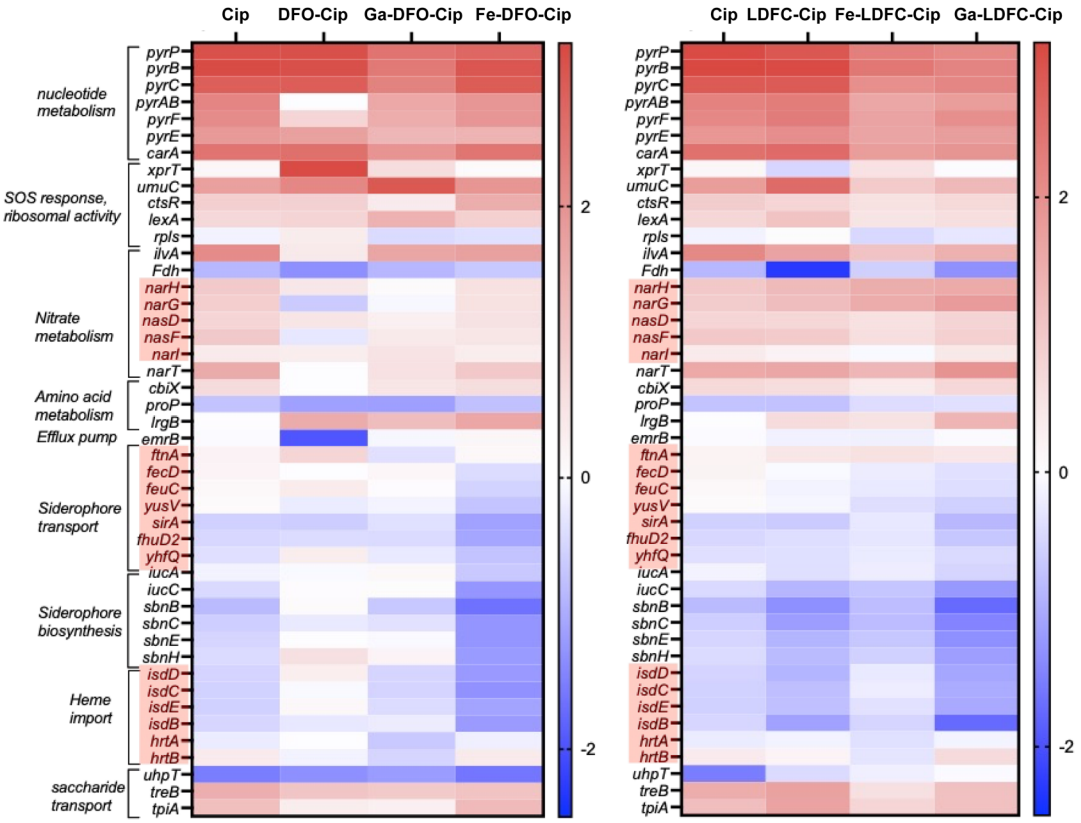


Fig. 5 Heat-map representation of differential gene expression in the presence of sub-$MIC_{98}$ quantities of sideromycins investigated in this study. Red refers to upregulated genes and blue to down-regulated genes within the heat map. Genes are grouped in accordance with their role within the bacterial organism. Genes in the red box require Fe-containing cofactors or substrates to execute function, such as Fe-heme, or Fe-complexed siderophores.

expression of the siderophore import machinery and iron storage (*fecDC* for **Ga–DFO–Cip** and *ftnA* for **Ga–LDFC–Cip**) contributes to the relative success of these compounds in internalization and growth inhibition.

### Differentially expressed genes in resistant *S. aureus* strains

We next pursued differential gene expression analysis in the three-resistance induced *S. aureus* strains. Fig. 6A displays the corresponding heat-map representation of differential gene expression. Purine biosynthesis (*pucG*) and amino-acid metabolism related proteins, such as *hisB*, *glnQ*, and *gltB*, are very significantly more down-regulated when compared in the **Ga–DFO–Cip** and **Ga–LDFC–Cip** resistant strains, when compared to the ciprofloxacin-resistant background. While none of these proteins contain Fe-cofactors or are known to correlate with iron homeostasis, histidine and glutamate are building blocks of *de novo* heme biosynthesis in *S. aureus*.[64–67] Further evidence for involvement of heme homeostasis is provided by the strongly upregulated *isdG* gene in **GaDFO–Cip**-resistant *S. aureus*, which encodes for a heme oxygenase that promotes the degradation of heme with subsequent release of iron. Simultaneous downregulation of bacterial ferritin (*ftn*) further indicates that the organism is using numerous mechanisms to mobilize cytoplasmic Fe(III).[68] Additional analysis of the transcriptional profile indicates that each resistant strain shares <40% commonly up- and down-regulated genes with the other two strains (Fig. 6B and C). In addition to well-characterized proteins, approximately 10% of proteins with unknown function were significantly contributing to the compound's unique transcriptomic signature.

### Mutations observed in ciprofloxacin, GaDFO–Cip and GaLDFC–Cip-resistant *S. aureus*

In addition to up- and downregulation of genes, we analyzed sequencing data to identify sites of mutations uniquely induced in each of the resistant strains when compared with the parent *wt S. aureus* strain. Using variant analysis, we identified SNPs (single nucleotide polymorphisms), insertions, deletions or structural variations (INDEL).[69] Fig. 7A–C list select unique and shared mutations for each resistant strain (for a complete list see also ESI Tables 5–7†). The mutations detected in the ciprofloxacin-resistant strain show numerous point mutations to ribosomal RNA (16S and 23S, entries 8 and 15) and a Snf2 like protein with helicase activity (Fig. 7A, entry 11).[70] Additionally, we also detected a single point mutation in an additional protein with sequence homology to helicases (Fig. 7A, entry 13). Of note, we did not observe mutation of topoisomerase which is a more typically observed resistance mechanism to

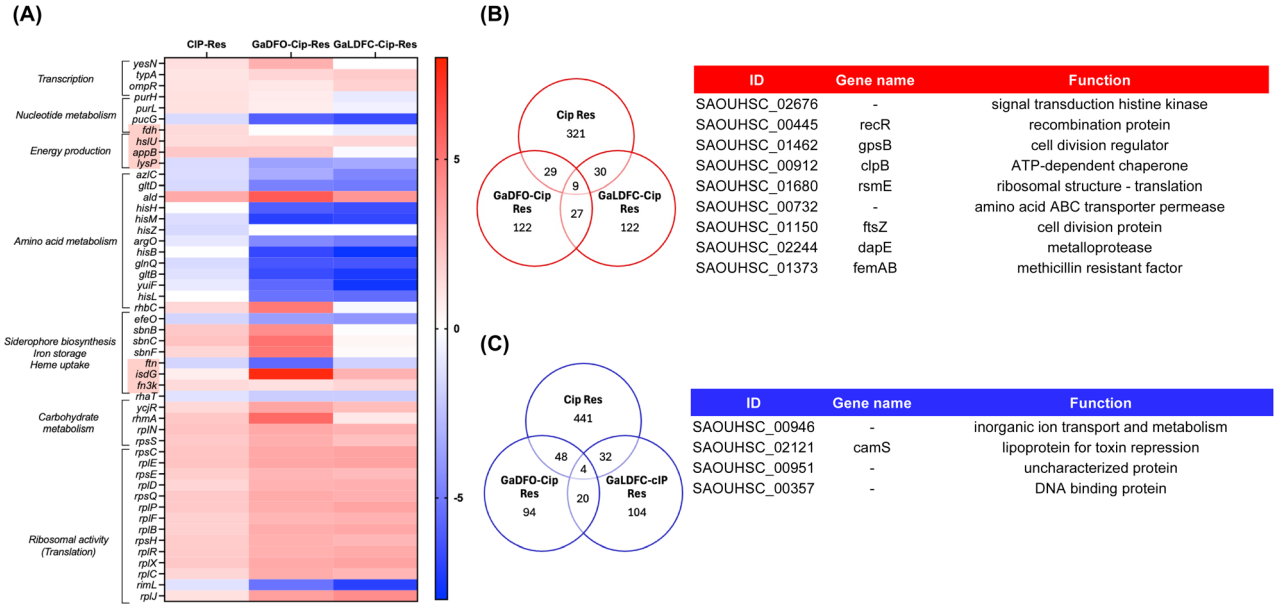


| ID | Gene name | Function |
|---|---|---|
| SAOUHSC_02676 | - | signal transduction histine kinase |
| SAOUHSC_00445 | recR | recombination protein |
| SAOUHSC_01462 | gpsB | cell division regulator |
| SAOUHSC_00912 | clpB | ATP-dependent chaperone |
| SAOUHSC_01680 | rsmE | ribosomal structure - translation |
| SAOUHSC_00732 | - | amino acid ABC transporter permease |
| SAOUHSC_01150 | ftsZ | cell division protein |
| SAOUHSC_02244 | dapE | metalloprotease |
| SAOUHSC_01373 | femAB | methicillin resistant factor |

| ID | Gene name | Function |
|---|---|---|
| SAOUHSC_00946 | - | inorganic ion transport and metabolism |
| SAOUHSC_02121 | camS | lipoprotein for toxin repression |
| SAOUHSC_00951 | - | uncharacterized protein |
| SAOUHSC_00357 | - | DNA binding protein |

Fig. 6 RNA-Seq analysis of the induced resistant strains. (A) Heat-map representation of differential gene expression in the resistant induced strains (*SACip-res*, *SAGaDFO-res*, and *SAGaLDFC-res*) compared to the *wt SA* strain. Red refers to upregulated genes and blue to down-regulated genes within the heat map. Genes are grouped in accordance with their role within the bacterial organism. Genes in the red box require Fe-containing cofactors or substrates to execute their function, such as Fe-heme or Fe-complexed siderophores. (B) Venn diagram and a table summarizing up-regulated genes in all three colonies that are above the set threshold of the analysis ($p$-value ≥ 0.05). (C) Venn diagram and a table summarizing down-regulated genes in all three colonies that are above the set threshold of the analysis ($p$-value ≥ 0.05).

(A) Cip-resistant

| Entry | ID | Type | Function |
|---|---|---|---|
| 1 | SAOUHSC_00275 | SNP | uncharacterized protein |
| 2 | SAOUHSC_00437 | SNP | trehalose specific IIBC component |
| 3 | SAOUHSC_00661 | SNP | lipid transport and metabolism |
| 4 | SAOUHSC_00275 | SNP | uncharacterized protein |
| 5 | SAOUHSC_T00018 | INDEL | tRNA-glu |
| 6 | SAOUHSC_00008 | SNP | histidine ammonia-lyase |
| 7 | SAOUHSC_01547 | INDEL | virulence-associated protein E |
| 8 | SAOUHSC_R0006 | SNP | 23S ribosomal RNA |
| 9 | SAOUHSC_02746 | SNP | hypothetical |
| 10 | SAOUHSC_02453 | SNP | tagatose-6-phosphate kinase |
| 11 | SAOUHSC_01542 | SNP | DNA, RNA helicase |
| 12 | SAOUHSC_01535 | INDEL | phage capside family |
| 13 | SAOUHSC_02476 | SNP | predicted helicase |
| 14 | SAOUHSC_01939 | INDEL | serine protease |
| 15 | SAOUHSC_R0001 | SNP | 16S ribosomal RNA |
| 16 | SAOUHSC_00544 | SNP | fibrinogen-binding protein |

(B) Ga-DFO-Cip-resistant

| Entry | ID | Type | Function |
|---|---|---|---|
| 17 | SAOUHSC_00653 | INDEL | ferrichrome transport permase fhuB, FecCD transport family |
| 18 | SAOUHSC_00765 | SNP | Replication, recombination and repair |
| 19 | SAOUHSC_00766 | INDEL | Predicted amidophosphoribosyltransferases |
| 20 | SAOUHSC_01512 | SNP | uncharacterized protein |
| 21 | SAOUHSC_00089 | INDEL | exopolysaccharide biosynthesis |
| 22 | SAOUHSC_R0002 | SNP | 16S ribosomal RNA |
| 23 | SAOUHSC_02866 | SNP | uncharacterized membrane protein |
| 24 | SAOUHSC_R00010 | SNP | 23S ribosomal RNA |
| 25 | SAOUHSC_02588 | SNP | uncharacterized protein |

(C) Ga-LDFC-Cip-resistant

| Entry | ID | Type | Function |
|---|---|---|---|
| | SAOUHSC_00094 | SNP | uncharacterized protein |
| 26 | SAOUHSC_00524 | SNP | rpoB DNA-directed RNA polymerase |
| 27 | SAOUHSC_01066 | SNP | protoheme IX farnesyltransferase |
| 28 | SAOUHSC_02127 | SNP | cysteine protease staphopain |
| 29 | SAOUHSC_00256 | INDEL | cell wall/membrane/envelope biogenesis |
| 30 | SAOUHSC_00471 | SNP | cell wall synthesis |
| 31 | SAOUHSC_00544 | INDEL | fibrinogen protein |
| 32 | SAOUHSC_00634 | SNP | ferric siderophore uptake |
| 33 | SAOUHSC_00152 | SNP | cysteine hydrolases |
| 34 | SAOUHSC_00509 | SNP | glutamyl tRNA |
| 35 | SAOUHSC_00643 | SNP | techoic acid bisynthesis protein |
| 36 | SAOUHSC_00129 | INDEL | cell wall/membrane/envelope biogenesis |
| 37 | SAOUHSC_00585 | SNP | uncharacterized protein |
| 38 | SAOUHSC_00515 | INDEL | rpoE, transcription |
| 39 | SAOUHSC_00118 | SNP | cell wall/membrane/envelope biogenesis, Posttranslational modification, protein turnover, chaperones |
| 40 | SAOUHSC_00304 | SNP | luciferase family oxidoreductase |
| 41 | SAOUHSC_00416 | SNP | membrane-associated lipid phosphatase |
| 42 | SAOUHSC_00552 | SNP | GlcN6P_deaminase |
| 43 | SAOUHSC_02767 | SNP | peptides uptake |
| 44 | SAOUHSC_00247 | SNP | cell wall/membrane/envelope biogenesis, |
| 45 | SAOUHSC_00113 | SNP | bifunctional acetaldehyde-CoA/alcohol dehydrogenase |
| 46 | SAOUHSC_00555 | SNP | energy production and conversion |
| 47 | SAOUHSC_00402 | SNP | staphylococcus tandem lipoproteins |
| 48 | SAOUHSC_00591 | INDEL | uncharacterized protein |
| 49 | SAOUHSC_00334 | SNP | ABC-2 family transporter protein |
| 50 | SAOUHSC_01087 | INDEL | ferric siderophore uptake (periplasmic domain) |
| 51 | SAOUHSC_00235 | SNP | carbohydrate transport and metabolism |
| 52 | SAOUHSC_00149 | SNP | arginine and lysine biosynthesis |
| 53 | SAOUHSC_00436 | SNP | glutamate synthase subunit beta; Reviewed |
| 54 | SAOUHSC_00190 | SNP | lipid transport and metabolism |
| 55 | SAOUHSC_00275 | SNP | unassigned protein |

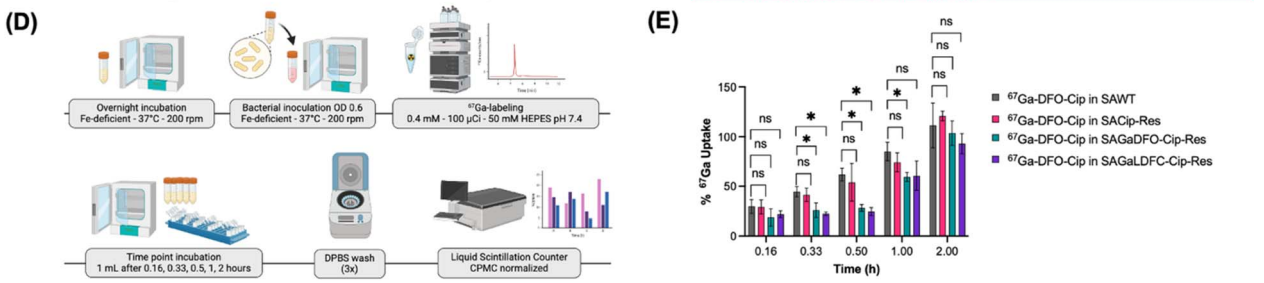


Fig. 7 Variants analysis. Top panel: table showing the unique variant in each resistant strain, (A) **Cip**-resistant, (B) **GaDFO–Cip**-resistant and (C) **GaLDFC–Cip**-resistant, that have quality above 100 and allele depth > 30. Bottom panel: (D) radiochemical bacterial uptake assay of $^{67}$**Ga–DFO–Cip** in *wt SA* and resistant *SA* under iron deficient conditions. (E) Quantification of radiolabeled $^{67}$**Ga-DFO-Cip** uptake in investigated strains shows decrease of accumulation sideromycin-resistan strains.

ciprofloxacin in *S. aureus*;[71] however, mutations that affect ribosome assembly have been implicated with exposure to multiple stressors (*e.g.* Fe-starvation and non-toxic levels of antibiotics) and may contribute to the evolution of high-level multidrug resistance.[72] Furthermore, other studies on induced resistance to ciprofloxacin have noted the absence of *gyrA* or *topB* mutations and instead report mutations of *rpoB*, *rpoE*, and parE, parC genes.[71] Indeed, the **Ga–LDFC–Cip**-resistant *S. aureus* strain shares a number of mutations with the ciprofloxacin-resistant strain (Fig. 7C, entries highlighted in pink) and shows emergence of *rpoB* (Fig. 7C, entry 26) and *rpoE* (Figure7C, entry 38 mutations, underscoring the compound's ciprofloxacin-like character). Other commonly shared mutation sites between the 3 strains encode for genes regulating lipid transport (Fig. 7A, entry 3; Fig. 7C, entry 54), fibrinogen binding protein (Fig. 7A, entry 16; Fig. 7C, entry 31), DNA binding (Fig. 7A, entry 5; Fig. 7C, entry 34) and cell wall biosynthesis (Fig. 7C, entries 29, 35, 39 and 44).

The lack of significant cross resistance to **Cip**, **Ga–DFO–Cip** and **Ga–LDFC–Cip** among the resistance-induced strains indicates a significant contribution from differential resistance profiles. Indeed, we identified several unique mutations in the **Ga–DFO–Cip** resistant and **Ga–LDFC–Cip** resistant strains. For **Ga–DFO–Cip** resistant *S. aureus*, we detected deletion of a 7-nucleotide fragment in a gene that encodes for *FhuB* (Fig. 7B, entry 17), a previously characterized ferrichrome/hydroxamate siderophore transporter.[13] The impaired FhuB transporter effectively decreases import of **Ga–DFO–Cip** and therefore reduces the compound's efficacy. We also observed the mutation of iron siderophore transport associated genes in the **Ga–LDFC–Cip** resistant *S. aureus* strain; however, instead of *FhuB*, which was unaffected, we observed mutations to two ABC transporter genes (Fig. 7C, entries 32 and 43), both are not yet well characterized, but are implicated in iron siderophore import. The absence of matching iron siderophore transporter mutations in the **Ga–DFO–Cip** and **Ga–LDFC–Cip** resistant strains explains the lack of pronounced cross-resistance of these compounds (Table 1). To affirm that these genes play a pivotal role in import of our synthetic sideromycins, we obtained *S. aureus* strains from the Nebraska Transposon Mutant Library, which contain transposon insertions into *S. aureus* genes of FhuB (SAOUHSC_00653) and the ferric siderophore uptake transporter (SAOUHSC_01087) to render the corresponding gene non-functional (equivalent to a knock-out mutation).[73] As anticipated, **Ga–DFO–Cip** and **Ga–LDFC–Cip** lost potency in both tested strains, while **Cip** retained moderate efficacy. This confirms that siderophore uptake machinery mutations are the bacteria's front-line resistance mechanism to xenometallomycins.

Additional single point mutations were also detected for the gene encoding for *cyoE*, protoheme IX farnesyltransferase (Fig. 7C, entry 27),[74] which is responsible for the incorporation of heme into membrane-associated electron transport cascades.[74,75] This mutation is further indicative of the role of Ga(III) in dysregulation of bacterial heme homeostasis and the bacteria's acute need for mobile iron sources within the cytoplasm. Additionally, we also detected a single point mutation in the serine protease gene, which prevents enzymatic release of

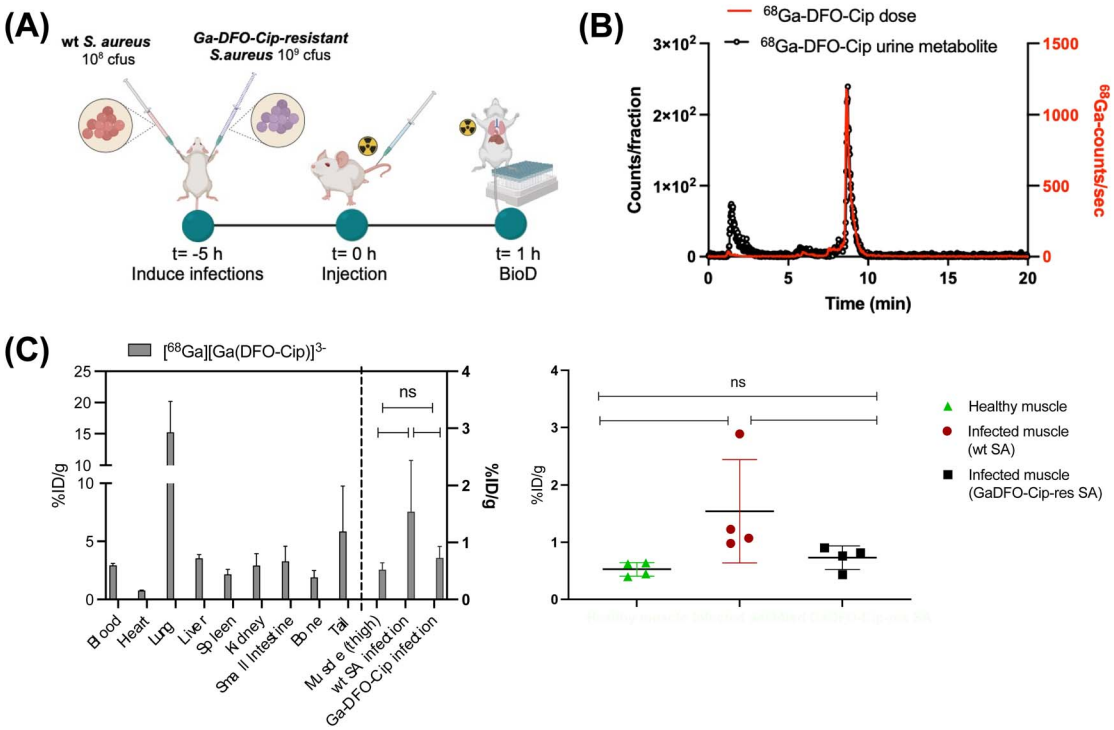


Fig. 8 *In vivo* biodistribution analysis in an infected model. (A) Workflow scheme, (B) urine metabolite analysis and (C) biodistribution of $[^{68}Ga][Ga(\textbf{DFO–Cip})]^{3-}$ in the infected model showing predominant accumulation in *wt SA* infected muscle compared to **GaDFO–Cip**-resistant infected muscle. **p* value = 0.037; ***p* value = 0.008.

ciprofloxacin from **Ga–LDFC–Cip** within the cytoplasm, further contributing to the resistance mechanism of **Ga–LDFC–Cip** resistant *S. aureus*. However, we consider neither one of these mutations as pivotal as transporter mutations to establish resistance.[76,77]

We hypothesized that **Ga–DFO–Cip** and **Ga–LDFC–Cip** resistance arise from impeded siderophore transport and therefore should significantly limit the uptake of the corresponding conjugates to the mutant bacterial cells. To probe this hypothesis, we conducted time-dependent radioactive uptake studies in *wt* and resistant strains using $^{67}$**Ga–DFO–Cip** (Fig. 7D). Quantification of $^{67}$**Ga–DFO–Cip** uptake within the bacterial pellets shows no difference in uptake in *wt* and **Cip**-resistant *S. aureus*; however, $^{67}$**Ga–DFO–Cip** uptake is repressed in **Ga–DFO–Cip** and **Ga–LDFC–Cip** resistant *S. aureus* strains (Fig. 7E). The persistent uptake indicates that the compounds can take advantage of multiple ports of entry, either by *FhuB* or the alternative ferric siderophore ABC transporter cascade implicated in **Ga–LDFC–Cip** resistance and mutants may retain a degree of functionality to translocate the conjugates, albeit with significantly reduced efficacy.

### *In vivo* biodistribution in an *wt S. aureus* infected model

We conducted an *in vivo* biodistribution assay in an infected mouse model (Fig. 8A) to determine the significance of siderophore transporter mutations in an *in vivo* environment. Localized soft tissue infections were induced in mice by injecting $10^8$ CFUs of *wt SA* into the right triceps and $10^8$ CFUs of the *SAGaDFO-Cip-resistant* bacteria into the contralateral left triceps.[31,35,78–81] After 5 hours, mice were intravenously injected with $^{68}$**Ga–DFO–Cip**, and biodistribution was assessed at 1 hour post-injection (Fig. 8A and B), alongside analysis of the metabolites in the urine (Fig. 8B). The biodistribution results revealed approximately 15% uptake of the conjugate in the lung, consistent with findings from previous studies on DFO-based conjugates and the enhanced uptake of ciprofloxacin in pulmonary tissue.[32,82] The $^{68}$**Ga–DFO–Cip** complex showed statistically significant, enhanced uptake in the *wt SA*-infected muscle compared to both the *SAGa-DFO-Cip-resistant* infected muscle and the control muscle, as shown in Fig. 8C. This selective uptake underscores the importance of active

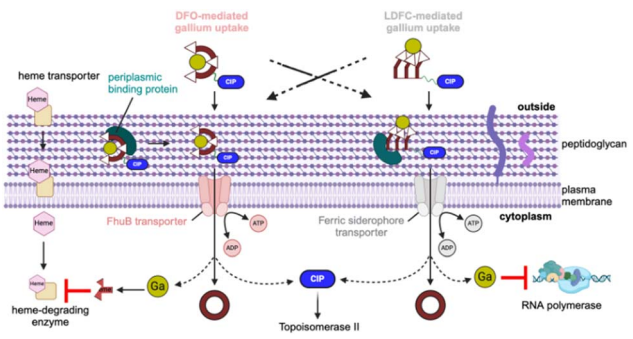


Fig. 9 Schematic representation of gallium–siderophore–ciprofloxacin conjugate uptake and its downstream effects in *S. aureus*.

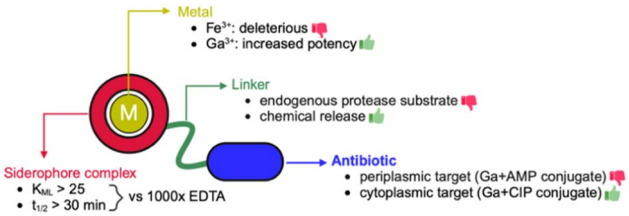


Fig. 10 Design criteria for the development of next generation siderophore–fluoroquinolone conjugates for inhibition of *S. aureus* growth.

transmembrane transport mediated uptake in live bacteria within the host. With the construct remaining >70%, the $^{68}$**Ga–DFO–Cip** probe dominates biological behavior over degradation and free $^{68}$Ga-mediated uptake (Fig. 8B).

## Conclusions

Here, we provide an exhaustive analysis and insight for the mechanism of action of gallium–siderophore conjugates and their ability to potentiate antibacterial activity of clinically employed antibiotic ciprofloxacin in *S. aureus* bacteria. Differential gene expression analysis of bacteria exposed to sub-MIC concentrations of the gallium–siderophore–ciprofloxacin conjugates reveals signatures characteristic of their parent antibiotic; compound import is facilitated by the bacteria's endogenous iron siderophore machinery, while import of alternative, common iron sources, such as Fe-heme, is repressed. Introduction of the corresponding iron analogues neutralizes Fe–siderophore import and rationalizes their low potency. We affirm the decreased growth inhibitory potency from Ga- to apo to Fe–siderophore–ampicillin conjugate and overall diminished potency relative to the parent antibiotic ampicillin.

*S. aureus* grown in the presence of sub-toxic, progressively increasing concentrations of the sideromycins, elicits mutations that confer enhanced tolerance to the corresponding compounds. Mutations of active, siderophore-complex mediated transport dominate the resistance mechanisms for both Ga-complexes evaluated, which is further affirmed by loss of potency in the corresponding, *S. aureus* knock-out mutants. In addition to ciprofloxacin-typical signatures, iron import and heme homeostasis become dysregulated; we also uncover that hydroxamate-based siderophores such as deferoxamine and desferrichrome use multiple transmembrane iron transport systems to access the bacterial cytoplasm of *S. aureus* bacterial strains (Fig. 9). Corresponding *in vitro* and *in vivo* experiments with the radioactive analogues $^{67/68}$**Ga–DFO–Cip** affirm that siderophore-specific transmembrane transport is essential to guarantee the delivery and uptake in *S. aureus* both outside and inside the mammalian host environment.

Taken together, our studies also outline design criteria for the future development of sideromycins as antibacterial agents for *S. aureus* (Fig. 10). Considering that Fe-complexes down-regulate expression of the siderophore uptake machinery, the use of apo- or Ga(III) complexes is preferable. The complex must

be sufficiently thermodynamically stable ($K_{ML}$ > 25) and kinetically inert ($t_{1/2}$ > 30 min *vs.* 1000-fold excess EDTA) to co-deliver metal ions and antibiotic cargo to the cytoplasm. Antibacterial cargos targeting the bacterial cell wall do not benefit significantly from co-delivery of a xenometal. Incorporation of siderophore antibiotic linkers that do not require degradation by endogenous bacterial proteases for activity but employ non-enzymatic release strategies may further prevent or delay emergence of resistance.

## Data availability

The datasets supporting this article have been uploaded as part of the ESI.† Specifically, we provide processed NMR spectroscopic information, chromatographic analysis spectra, UV-vis spectra and tabulated biodistribution and stability analysis data as an average of single cohorts of animals as indicated. Tabulated raw RNA-Seq data are provided as supplementary Excel files. Additional raw data are available upon request to the corresponding author.

## Author contributions

EB, AM designed and planned experiments. AM, OG, JEH, MC conducted experiments and contributed to data analysis. EB and AM conducted data analysis and interpretation. The manuscript and supporting information was written with contributions from all authors.

## Conflicts of interest

There are no conflicts to declare.

## Acknowledgements

The National Institute of General Medical Sciences (NIGMS) is acknowledged for funding (R35GM142770). The authors utilized the University of Wisconsin-Madison Biotechnology Center Bioinformatics Core Facility (Research Resource Identifier – RRID:SCR_017799) for analysis of differentially expressed genes in the wild-type *S. aureus* bacteria in response to the compounds and in the induced resistant *S. aureus* as well the variant analysis of the resistant strains. Dr Mark Berres is acknowledged for his support in RNA sequencing data processing and analysis. Dr Heike Hofstetter is acknowledged for her support in establishing various heteronuclear NMR pulse programs and acquisition methods. The following instrumentation in the Paul Bender Chemical Instrumentation Center at the University of Wisconsin-Madison was supported by NSF CHE-2017891 (Bruker Avance Neo 500); by a generous gift from Paul J. and Margaret M. Bender (Bruker Quazar APEX2 and Bruker 500); NIH S10 OD012245 (Bruker Avance-600). The Electrospray Ionization-Quadrupole-Ion Trap Mass Spectrometer was funded by NIH 1S10 OD020022. Z. Rosenkrans, staff at Small Animal Imaging and Radiotherapy Facility (SAIRF) is acknowledged for tail vein injection during the *in vivo* study.

## References

1 E. Lappin and A. J. Ferguson, *Lancet Infect. Dis.*, 2009, **9**, 281–290.
2 G. H. Dayan, N. Mohamed, I. L. Scully, D. Cooper, E. Begier, J. Eiden, K. U. Jansen, A. Gurtman and A. S. Anderson, *Expert Rev. Vaccines*, 2016, **15**, 1373–1392.
3 V. Pintado, R. Pazos, M. E. Jiménez-Mejías, A. Rodríguez-Guardado, B. Díaz-Pollán, C. Cabellos, J. M. García-Lechuz, J. Lora-Tamayo, P. Domingo, E. Muñez, D. Domingo, F. González-Romo, J. A. Lepe-Jiménez, C. Rodríguez-Lucas, A. Gil, I. Pelegrín, F. Chaves, V. Pomar, A. Ramos, T. Alarcón and E. Pérez-Cecilia, *J. Hosp. Infect.*, 2019, **102**, 108–115.
4 S. Y. C. Tong, J. S. Davis, E. Eichenberger, T. L. Holland and V. G. Fowler, *Clin. Microbiol. Rev.*, 2015, **28**, 603–661.
5 T. J. Foster, *FEMS Microbiol. Rev.*, 2017, **41**, 430–449.
6 Y. Guo, G. Song, M. Sun, J. Wang and Y. Wang, *Front. Cell. Infect. Microbiol.*, 2020, **10**, DOI: 10.3389/fcimb.2020.00107.
7 A. M. Timofeeva, M. R. Galyamova and S. E. Sedykh, *Plants*, 2022, **11**, 3065.
8 B. Rayner, A. D. Verderosa, V. Ferro and M. A. T. Blaskovich, *RSC Med. Chem.*, 2023, **14**, 800–822.
9 V. Braun, *Front. Biosci.*, 2003, **8**, s1409–s1421.
10 J. E. Cassat and E. P. Skaar, *Semin. Immunopathol.*, 2012, **34**, 215–235.
11 T. E. Clarke, L. W. Tari and H. J. Vogel, *Curr. Top. Med. Chem.*, 2001, **1**, 7–30.
12 B. S. Conroy, J. C. Grigg, M. Kolesnikov, L. D. Morales and M. E. P. Murphy, *BioMetals*, 2019, **32**, 409–424.
13 M. T. Sebulsky, B. H. Shilton, C. D. Speziali and D. E. Heinrichs, *J. Biol. Chem.*, 2003, **278**, 49890–49900.
14 A. Stintzi, C. Barnes, J. Xu and K. N. Raymond, *Proc. Natl. Acad. Sci. U. S. A.*, 2000, **97**, 10691–10696.
15 M. C. van Dijk, R. M. de Kruijff and P.-L. Hagedoorn, *Front. Cell Dev. Biol.*, 2022, **10**, 857237.
16 T. Zheng, J. L. Bullock and E. M. Nolan, *J. Am. Chem. Soc.*, 2012, **134**, 18388–18400.
17 C. Ji and M. J. Miller, *BioMetals*, 2015, **28**, 541–551.
18 K. S. Kaye, T. Naas, J. M. Pogue and G. M. Rossolini, *Infect. Dis. Ther.*, 2023, **12**, 777–806.
19 K. A. Parsels, K. A. Mastro, J. M. Steele, S. J. Thomas and W. D. Kufel, *J. Antimicrob. Chemother.*, 2021, **76**, 1379–1391.
20 J. Yao, J. Wang, M. Chen and Y. Cai, *Front. Med.*, 2021, **8**, DOI: 10.3389/fmed.2021.741940.
21 A. Sollima, F. Rossini, P. Lanza, C. Pallotto, M. Meschiari, I. Gentile, R. Stellini, A. Lenzi, A. Mulé, F. Castagna, S. Lorenzotti, S. Amadasi, E. Van Hauwermeiren, B. Saccani, B. Fumarola, L. Signorini, F. Castelli and A. Matteelli, *Antibiotics*, 2024, **13**, 453.
22 G. J. Anderson and D. M. Frazer, *Am. J. Clin. Nutr.*, 2017, **106**, 1559S–1566S.
23 E. R. Frawley and F. C. Fang, *Mol. Microbiol.*, 2014, **93**, 609–616.
24 C. R. Chitambar, *Biochim. Biophys. Acta, Mol. Cell Res.*, 2016, **1863**, 2044–2053.

25 N. Kircheva and T. Dudev, *Inorg. Chem.*, 2020, **59**, 6242–6254.
26 S. Hijazi, D. Visaggio, M. Pirolo, E. Frangipani, L. Bernstein and P. Visca, *Front. Cell. Infect. Microbiol.*, 2018, **8**, 316.
27 K. D. Mjos, J. F. Cawthray, E. Polishchuk, M. J. Abrams and C. Orvig, *Dalton Trans.*, 2016, **45**, 13146–13160.
28 K. Michalska, M. Rychłowski, M. Krupińska, G. Szewczyk, T. Sarna and J. Nakonieczna, *Mol. Pharm.*, 2022, **19**, 1434–1448.
29 Z. W. Scott, S. Choi, B. E. Britigan and P. Narayanasamy, *ACS Infect. Dis.*, 2023, **9**, 716–738.
30 R. G. Pearson, *J. Org. Chem.*, 1989, **54**, 1423–1430.
31 A. Pandey, D. Śmiłowicz and E. Boros, *Chem. Sci.*, 2021, **12**, 14546–14556.
32 A. Pandey, C. Savino, S. H. Ahn, Z. Yang, S. G. Van Lanen and E. Boros, *J. Med. Chem.*, 2019, **62**, 9947–9960.
33 V. Vinuesa and M. J. McConnell, *Int. J. Mol. Sci.*, 2021, **22**, 2876.
34 Y. Wang, B. Han, Y. Xie, H. Wang, R. Wang, W. Xia, H. Li and H. Sun, *Chem. Sci.*, 2019, **10**, 6099–6106.
35 A. Pandey, M. Cao and E. Boros, *ACS Infect. Dis.*, 2022, **8**, 878–888.
36 X. S. Pan, J. Ambler, S. Mehtar and L. M. Fisher, *Antimicrob. Agents Chemother.*, 1996, **40**, 2321–2326.
37 K. A. Gould, X.-S. Pan, R. J. Kerns and L. M. Fisher, *Antimicrob. Agents Chemother.*, 2004, **48**, 2108–2115.
38 K. M. Evans-Roberts, L. A. Mitchenall, M. K. Wall, J. Leroux, J. S. Mylne and A. Maxwell, *J. Biol. Chem.*, 2016, **291**, 3136–3144.
39 A. R. Cardoso, L. P. T. Carneiro, G. Cabral-Miranda, M. F. Bachmann and M. G. F. Sales, *Chem. Eng. J.*, 2021, **409**, 128135.
40 A. Ito, T. Nishikawa, S. Matsumoto, H. Yoshizawa, T. Sato, R. Nakamura, M. Tsuji and Y. Yamano, *Antimicrob. Agents Chemother.*, 2016, **60**, 7396–7401.
41 T. Emery and P. B. Hoffer, *J. Nucl. Med.*, 1980, **21**, 935–939.
42 A. Evers, R. D. Hancock, A. E. Martell and R. J. Motekaitis, *Inorg. Chem.*, 1989, **28**, 2189–2195.
43 N. P. Endicott, E. Lee and T. A. Wencewicz, *ACS Infect. Dis.*, 2017, **3**, 542–553.
44 M. I. Tsionou, C. E. Knapp, C. A. Foley, C. R. Munteanu, A. Cakebread, C. Imberti, T. R. Eykyn, J. D. Young, B. M. Paterson, P. J. Blower and M. T. Ma, *RSC Adv.*, 2017, **7**, 49586–49599.
45 N. Mani, C. H. Gross, J. D. Parsons, B. Hanzelka, U. Müh, S. Mullin, Y. Liao, A.-L. Grillot, D. Stamos, P. S. Charifson and T. H. Grossman, *Antimicrob. Agents Chemother.*, 2006, **50**, 1228–1237.
46 J. R. Anderson, N. B. Lam, J. L. Jackson, S. M. Dorenkott, T. Ticer, E. Maldosevic, A. Velez, M. R. Camden and T. N. Ellis, *Antibiotics*, 2023, **12**, 887.
47 N. Kuptsov, M. Kornienko, D. Bespiatykh, R. Gorodnichev, K. Klimina, V. Veselovsky and E. Shitikov, *Viruses*, 2022, **14**, 567.
48 J. Im, D. Lee, O.-J. Park, S. Natarajan, J. Park, C.-H. Yun and S. H. Han, *Front. Microbiol.*, 2022, **13**, DOI: **10.3389/fmicb.2022.1063650**.
49 L. Bie, M. Zhang, J. Wang, M. Fang, L. Li, H. Xu and M. Wang, *Microbiol. Spectr.*, 2023, **11**, e00317–e00323.
50 N. J. Croucher and N. R. Thomson, *Curr. Opin. Microbiol.*, 2010, **13**, 619–624.
51 D. Trivier and R. J. Courcol, *FEMS Microbiol. Lett.*, 1996, **141**, 117–127.
52 I. Z. Batko, R. S. Flannagan, V. Guariglia-Oropeza, J. R. Sheldon and D. E. Heinrichs, *J. Bacteriol.*, 2021, **203**, DOI: **10.1128/jb.00458-21**.
53 M. Allard, H. Moisan, É. Brouillette, A. L. Gervais, M. Jacques, P. Lacasse, M. S. Diarra and F. Malouin, *Microb. Infect.*, 2006, **8**, 1679–1690.
54 K. P. Ha and A. M. Edwards, *Microbiol. Mol. Biol. Rev.*, 2021, **85**, DOI: **10.1128/MMBR.00091-21**.
55 L. C. N. da Silva, R. C. Diniz, I. M. d. S. F. Lima, C. I. dos Santos, M. S. Alves, L. I. O. de Souza and A. d. S. Monteiro, in *The Rise of Virulence and Antibiotic Resistance in Staphylococcus aureus*, IntechOpen, 2017.
56 K. H. Maslowska, K. Makiela-Dzbenska and I. J. Fijalkowska, *Environ. Mol. Mutagen.*, 2019, **60**, 368–384.
57 J. Y. Park, J. W. Kim, B. Y. Moon, J. Lee, Y. J. Fortin, F. W. Austin, S.-J. Yang and K. S. Seo, *Infect. Immun.*, 2015, **83**, 1620–1628.
58 A. Y. Bhagirath, Y. Li, R. Patidar, K. Yerex, X. Ma, A. Kumar and K. Duan, *Int. J. Mol. Sci.*, 2019, **20**, 1781.
59 M. G. Bertero, R. A. Rothery, M. Palak, C. Hou, D. Lim, F. Blasco, J. H. Weiner and N. C. J. Strynadka, *Nat. Struct. Mol. Biol.*, 2003, **10**, 681–687.
60 Y. Dong, X. Miao, Y.-D. Zheng, J. Liu, Q.-Y. He, R. Ge and X. Sun, *J. Proteome Res.*, 2021, **20**, 2839–2850.
61 L. R. Mesak, V. Miao and J. Davies, *Antimicrob. Agents Chemother.*, 2008, **52**, 3394–3397.
62 S. P. Mattiello, V. C. Barth, J. Scaria, C. a. S. Ferreira and S. D. Oliveira, *Sci. Rep.*, 2023, **13**, 18696.
63 A. A. Pometun, K. M. Boyko, T. S. Yurchenko, A. Y. Nikolaeva, I. S. Kargov, D. L. Atroshenko, S. S. Savin, V. O. Popov and V. I. Tishkov, *Biochemistry*, 2020, **85**, 689–696.
64 G. A. Ashniev, N. V. Sernova, A. E. Shevkoplias, I. D. Rodionov, I. A. Rodionova, A. G. Vitreschak, M. S. Gelfand and D. A. Rodionov, *BMC Genom.*, 2022, **23**, 558.
65 C. M. Beetham, C. F. Schuster, I. Kviatkovski, M. Santiago, S. Walker and A. Gründling, *PLoS Pathog.*, 2024, **20**, e1011927.
66 T. Saito, D. Duly and R. J. Williams, *Eur. J. Biochem.*, 1991, **197**, 39–42.
67 H. H. Brewitz, N. Goradia, E. Schubert, K. Galler, T. Kühl, B. Syllwasschy, J. Popp, U. Neugebauer, G. Hagelueken, O. Schiemann, O. Ohlenschläger and D. Imhof, *Biochim. Biophys. Acta, Gen. Subj.*, 2016, **1860**, 1343–1353.
68 L. J. Lojek, A. J. Farrand, A. Weiss and E. P. Skaar, *Int. J. Med. Microbiol.*, 2018, **308**, 582–589.
69 N. D. Olson, J. Wagner, N. Dwarshuis, K. H. Miga, F. J. Sedlazeck, M. Salit and J. M. Zook, *Nat. Rev. Genet.*, 2023, **24**, 464–483.
70 D. P. Ryan and T. Owen-Hughes, *Curr. Opin. Chem. Biol.*, 2011, **15**, 649–656.

71 D. Ince and D. C. Hooper, *J. Bacteriol.*, 2003, **185**, 6883–6892.
72 J. E. Gomez, B. B. Kaufmann-Malaga, C. N. Wivagg, P. B. Kim, M. R. Silvis, N. Renedo, T. R. Ioerger, R. Ahmad, J. Livny, S. Fishbein, J. C. Sacchettini, S. A. Carr and D. T. Hung, *eLife*, 2017, **6**, e20420.
73 P. D. Fey, J. L. Endres, V. K. Yajjala, T. J. Widhelm, R. J. Boissy, J. L. Bose and K. W. Bayles, *mBio*, 2013, **4**, DOI: **10.1128/mbio.00537-12**.
74 E. Stevens, M. Laabei, S. Gardner, G. A. Somerville and R. C. Massey, *Sci. Rep.*, 2017, **7**, 13744.
75 T. Xu, J. Han, J. Zhang, J. Chen, N. Wu, W. Zhang and Y. Zhang, *Front. Microbiol.*, 2016, **7**, 1625.
76 K. Stelzner, A. Boyny, T. Hertlein, A. Sroka, A. Moldovan, K. Paprotka, D. Kessie, H. Mehling, J. Potempa, K. Ohlsen, M. J. Fraunholz and T. Rudel, *PLoS Pathog.*, 2021, **17**, e1009874.
77 K. Rice, R. Peralta, D. Bast, J. de Azavedo and M. J. McGavin, *Infect. Immun.*, 2001, **69**, 159–169.
78 K. Krasulova, B. Neuzilova, K. D. Bendova, Z. Novy, M. Popper, M. Hajduch and M. Petrik, *EJNMMI Radiopharm. Chem.*, 2024, **9**, 20.
79 C. Peukert, L. N. B. Langer, S. M. Wegener, A. Tutov, J. P. Bankstahl, B. Karge, F. M. Bengel, T. L. Ross and M. Brönstrup, *J. Med. Chem.*, 2021, **64**, 12359–12378.
80 M. Petrik, E. Umlaufova, V. Raclavsky, A. Palyzova, V. Havlicek, J. Pfister, C. Mair, Z. Novy, M. Popper, M. Hajduch and C. Decristoforo, *Eur. J. Nucl. Med. Mol. Imaging*, 2021, **48**, 372–382.
81 G. Narayanappa and B. N. Nandeesh, *Brain Pathol.*, 2021, **31**, e12950.
82 H. X. Ong, D. Traini, M. Bebawy and P. M. Young, *Antimicrob. Agents Chemother.*, 2013, **57**, 2535–2540.